Draft version February 20, 2015
Preprint typeset using LaTeX style emulateapj v. 5/2/11

arXiv:1408.1092v2 [astro-ph.GA] 19 Feb 2015

HALF OF THE MOST LUMINOUS QUASARS MAY BE OBSCURED: INVESTIGATING THE NATURE OF WISE-SELECTED HOT, DUST-OBSCURED GALAXIES

R.J. Assef[1], P.R.M. Eisenhardt[2], D. Stern[2], C.-W. Tsai[2,3], J. Wu[4], D. Wylezalek[5], A.W. Blain[6], C.R. Bridge[7]
E. Donoso[8], A. Gonzales[7,9,10], R.L. Griffith[11], T.H. Jarrett[12]

Draft version February 20, 2015

ABSTRACT

The WISE mission has unveiled a rare population of high-redshift ($z = 1 - 4.6$), dusty, hyper-luminous galaxies, with infrared luminosities $L_{\rm IR} > 10^{13}\ L_{\odot}$, and sometimes exceeding $10^{14}\ L_{\odot}$. Previous work has shown that their dust temperatures and overall far-IR spectral energy distributions (SEDs) are significantly hotter than expected to be powered by star-formation. We present here an analysis of the rest-frame optical through mid-IR SEDs for a large sample of these so-called "Hot, Dust-Obscured Galaxies" (Hot DOGs). We find that the SEDs of Hot DOGs are generally well modeled by the combination of a luminous, yet obscured AGN that dominates the rest-frame emission at $\lambda > 1\mu$m and the bolometric luminosity output, and a less luminous host galaxy that is responsible for the bulk of the rest optical/UV emission. Even though the stellar mass of the host galaxies may be as large as $10^{11} - 10^{12}\ M_{\odot}$, the AGN emission, with a range of luminosities comparable to those of the most luminous QSOs known, require that either Hot DOGs have black hole masses significantly in excess of the local relations, or that they radiate significantly above the Eddington limit, at a level at least 10 times more efficiently than $z \sim 2$ QSOs. We show that, while rare, the number density of Hot DOGs is comparable to that of equally luminous but unobscured (i.e., Type 1) QSOs. This may be at odds with the trend suggested at lower luminosities for the fraction of obscured AGN to decrease with increasing luminosity. That trend may, instead, reverse at higher luminosities. Alternatively, Hot DOGs may not be the torus-obscured counterparts of the known optically selected, largely unobscured Hyper-Luminous QSOs, and may represent a new component of the galaxy evolution paradigm. Finally, we discuss the environments of Hot DOGs and statistically show that these objects are in regions as dense as those of known high-redshift proto-clusters.

Subject headings: galaxies: active — galaxies: evolution — galaxies: high-redshift — quasars: general — infrared: galaxies

1. INTRODUCTION

Massive galaxies are thought to evolve from star-forming disks into passive ellipticals through major mergers that trigger star-formation and intense episodes of accretion into their central super-massive black holes (SMBHs) (e.g. Hopkins et al. 2008). Such a picture can explain several properties of galaxies, such as the tight correlations between the mass of their SMBH ($M_{\rm BH}$) and the mass, luminosity and velocity dispersion of the galaxy's spheroidal component (e.g. Magorrian et al. 1998; Ferrarese & Merritt 2000; Tremaine et al. 2002; Marconi & Hunt 2003; Bentz et al. 2009; Gültekin et al. 2009), and the evolution of the galaxy luminosity density (e.g., Faber et al. 2007). In these scenarios, the host galaxy stellar mass is assembled through star-formation ahead of the onset of the active galactic nuclei (AGN), which through a feedback mechanism heats up the gas and expels some of it, thereby quenching its star-formation.

An important characteristic of both the intense star-formation and AGN episodes is the significant quantities of dust associated with them. In galaxies undergoing extreme star-formation and AGN activity, a large fraction of the luminous energy is absorbed by dust and then re-radiated at infrared/sub-mm wavelengths, as observed for populations such as Ultra-Luminous Infrared Galaxies (ULIRGs; Sanders & Mirabel 1996), Sub-mm Galaxies (SMGs; Blain et al. 2002; Casey et al. 2014) and Dust-Obscured Galaxies (DOGs; Dey et al. 2008). It follows then that studying the most luminous infrared galaxies in the Universe, which host the most intense star-formation and AGN activity, likely probe extreme scenarios within the galaxy evolution paradigm.

[1] Núcleo de Astronomía de la Facultad de Ingeniería, Universidad Diego Portales, Av. Ejército Libertador 441, Santiago, Chile. E-mail: roberto.assef@mail.udp.cl
[2] Jet Propulsion Laboratory, California Institute of Technology, 4800 Oak Grove Drive, Pasadena, CA 91109, USA.
[3] NASA Postdoctoral Program Fellow
[4] UCLA Astronomy, PO Box 951547, Los Angeles, CA 90095-1547, USA
[5] European Southern Observatory, Karl-Schwarzschildstr.2, D-85748 Garching bei München, Germany
[6] Physics & Astronomy, University of Leicester, 1 University Road, Leicester LE1 7RH, UK
[7] Division of Physics, Math, and Astronomy, California Institute of Technology, Pasadena, CA 91125, USA
[8] Instituto de Ciencias Astronómicas, de la Tierra, y del Espacio (ICATE), 5400, San Juan, Argentina
[9] Department of Earth, Atmospheric and Planetary Sciences, Massachusetts Institute of Technology, Cambridge, MA 02139, USA
[10] Scripps College, 1030 Columbia Avenue, Claremont, CA 91711, USA
[11] Department of Astronomy and Astrophysics, The Pennsylvania State University, 525 Davey Lab, University Park, PA 16802, USA
[12] Astrophysics, Cosmology and Gravity Centre (ACGC), Astronomy Department, University of Cape Town, Private Bag X3, Rondebosch 7701, South Africa

NASA's Wide-field Infrared Survey Explorer (WISE; Wright et al. 2010) was launched in December 2009, and surveyed the entire sky in four mid-IR bands centered at 3.4μm (W1), 4.6μm (W2), 12μm (W3) and 22μm (W4). One of the main goals of the WISE mission was to identify the most luminous infrared galaxies in the universe, and the mission has achieved considerable success towards this goal in the past few years (Eisenhardt et al. 2012; Wu et al. 2012; Bridge et al. 2013; Jones et al. 2014; Stern et al. 2014; Wu et al. 2014; Eisenhardt et al. in prep.; Lonsdale et al. in prep.; Tsai et al. 2014). One highly successful method to identify such sources is to target objects that are extremely red in the WISE bands, with faint or no detections in the more sensitive W1 and W2 bands, but well detected in W3 and W4. These selection criteria were presented by Eisenhardt et al. (2012) and have been shown to successfully identify a population of luminous galaxies with $z \gtrsim 1$ (for details on the selection criteria, see Eisenhardt et al. 2012, and §2.1). Using sub-mm observations, Wu et al. (2012) showed that these objects are indeed extremely luminous, with bolometric luminosities exceeding 10^{13} $L_{\odot}$, and sometimes exceeding 10^{14} $L_{\odot}$. These observations also showed that the dust in these objects is at temperatures significantly higher than in other luminous infrared populations, such as ULIRGs and SMGs, peaking at rest-frame wavelengths $\lambda \lesssim 20\mu$m. Such high dust temperatures are consistent with AGN heating, suggesting the bulk of the luminosity is produced by accretion onto the galaxy's central SMBH rather than by star-formation. Indeed, Eisenhardt et al. (2012) in a detailed study of one of these sources, WISE J181417.29+341224.9 (W1814+3412 hereafter), determined that its spectral energy distribution (SED) is consistent with a heavily obscured ($A_V \sim 50$ mag) AGN producing the bulk of the luminosity. Due to their high dust temperatures, and yet similar optical-to-mid-IR colors to DOGs, we adopt the terminology of Wu et al. (2012) and refer to these objects as Hot, Dust-Obscured Galaxies or Hot DOGs.

Follow-up studies have provided additional interesting aspects of this population. The observed-frame optical spectra of these objects (Eisenhardt et al. 2012; Wu et al. 2012; Stern et al. 2014; Eisenhardt et al. in prep.) have diverse properties. While many of these objects show narrow emission lines commonly associated with obscured AGN activity present in the IR, some show features more closely associated with star-formation, with mostly absorption lines and only Lyα emission (e.g., W1814+3412 Eisenhardt et al. 2012), and some even show red continua with a lack of emission lines (e.g.,WISE J092625.44+423251.9; Wu et al. 2012). Imaging obtained with the *Hubble Space Telescope*/WFC3 and through adaptive optics with Keck/NIRC2 have shown that these objects typically are not gravitationally lensed, implying their luminosities are intrinsic (Eisenhardt et al. 2012; Wu et al. 2014; Tsai et al. 2014). Recently, Jones et al. (2014) reported observations at 850μm with SCUBA-2 at the James Clerk Maxwell Telescope (JCMT) of a subsample of 10 Hot DOGs, which suggest these objects are located in arcmin-scale overdensities of luminous dusty galaxies (see §6) and confirm the hot dust temperatures determined by Wu et al. (2012). Jones et al. (2014) constrain the contribution of ULIRG-type star-formation to less than 30% of the IR luminosity, and of spiral-type star-formation to less than 3%. Similar conclusions are reached by Wu et al. (2014), who studied two Hot DOGs at submm and mm wavelengths at higher spatial resolution using the Submillimeter Array (SMA) and the Combined Array for Research in Millimeter-wave Astronomy (CARMA). Wu et al. (2014) was able to constrain their cold dust masses to amounts comparable to those of quasars with comparable luminosities. On the other end of the electromagnetic spectrum, Stern et al. (2014) studied the AGN nature of three Hot DOGs using X-ray observations obtained with the *X-ray Multi-Mirror Mission* (*XMM-Newton*) and the *Nuclear Spectroscopic Telescope Array* (*NuSTAR*), finding that the AGN emission is heavily absorbed, possibly Compton-thick. Using a similar sample to that defined by the Hot DOG selection criteria, Bridge et al. (2013) determined that a significant fraction of such objects show extended Lyα emission on 30 – 100 kpc scales, and pointed out this could be consistent with the presence of intense quasar feedback. Bridge et al. (2013) also further constrained the high temperature of these objects by using *Herschel*/PACS and SPIRE observations to map the full shape of their far-IR SEDs. Finally, Lonsdale et al. (in prep.) present a study based on ALMA Cycle 0 observations of the far-IR SEDs of radio-selected, red WISE objects that are possibly the radio-loud counterparts of Hot DOGs. Although these objects are located at somewhat lower redshifts (0.47–2.85), they share some of the same characteristics, including the overall high dust temperatures and an even more dramatic apparent overdensity of nearby luminous dusty galaxies (Jones et al. in prep.).

In this work we study the physical properties of Hot DOGs by analyzing their SEDs, number densities and environments. In a companion paper, Tsai et al. (2014) presents a detailed study of the most luminous Hot DOGs, those with bolometric luminosities in excess of 10^{14} $L_{\odot}$. The article is structured as follows. In Section 2 we discuss the sample selection and the follow-up photometric and spectroscopic observations. In Section 3 we present our SED modeling methodology, while in Section 4 we apply it to model our sample of Hot DOGs and discuss their inferred physical properties. In Section 5 we compare the number density of Hot DOGs to that of comparably luminous QSOs. Finally, in Section 6 we study the density of the environments in which Hot DOGs are found using follow-up *Warm Spitzer*/IRAC imaging. We discuss how the environments compare to known clusters at similar redshifts, and how this constrains the stellar masses of Hot DOGs. Throughout this work we assume a flat ΛCDM cosmology with $H_0 = 73$ km s^{-1}, $\Omega_M = 0.3$, and $\Omega_{\Lambda} = 0.7$. We refer to all magnitudes in the Vega photometric system. For convenience, the different samples used throughout this work are summarized in Table 1.

2. SAMPLE SELECTION AND MULTI-WAVELENGTH FOLLOW-UP OBSERVATIONS

2.1. *WISE and the W12drop Selection*

The WISE mission observed the full sky in four mid-IR photometric bands with a FWHM of 6″ in W1–3 and 12″ in W4. We use the WISE All-Sky data release, which includes all observations obtained during the fully cryogenic mission. WISE surveyed the sky in a polar or-

Table 1
Sample Definition

Sample	Description	*All*		*IRAC Detected*	
		N	Nz	N	Nz
Full Sample W12drop	Eqn. (1)	934	155	711	115
Full Sample Hot DOG	$z > 1$ and W12drop	···	122	···	96
Core Sample W12drop	W4<7.2 and W12drop	252	95	103	58
Core Sample Hot DOG	W4<7.2 and Hot DOG	···	77	···	52
Hot DOGs for number density analysis (§5)	$2 < z < 4$ and Core Sample Hot DOG	···	···	···	42

Note. — All results presented in this article are based on objects detected by *Warm Spitzer*/IRAC (see §2.2.1). The definition of the Hot DOG population presented in this table reflects the definition adopted for this work but is somewhat more restrictive than those used elsewhere (e.g., as in Wu et al. 2012; see §4). Note that for samples where z is not required for their selection, N is the total number of objects regardless of whether they have been observed spectroscopically, while Nz shows the number of objects with a measured redshift.

bit with respect to the ecliptic, simultaneously obtaining images in all four bands. Hence, the number of observations in a field increases with its ecliptic latitude. While fields near the ecliptic were typically observed 12 times, the number can grow to thousands near the ecliptic poles (e.g., Jarrett et al. 2011). The median coverage across the sky is approximately 15 frames per passband. Detailed accounts of the mission are presented by Wright et al. (2010) and in the WISE All-Sky data release explanatory supplement[13].

As discussed earlier, our canonical picture of galaxy evolution suggests the existence of key stages where massive galaxies experience extremely luminous but heavily dust-enshrouded star-formation and nuclear activity. For the most massive galaxies, these stages may reach infrared luminosities $L_{\rm IR} > 10^{13}\ L_{\odot}$, and hence be classified as Hyper-Luminous Infrared Galaxies (HyLIRGs), but can be very faint in the optical bands due to obscuration. Wu et al. (2012) and Eisenhardt et al. (2012) presented a large sample of WISE-selected HyLIRGs, which are the main target of this study. The selection criteria used by Eisenhardt et al. (2012) and Wu et al. (2012) specifically target galaxies red enough to be well detected in the long wavelength WISE bands W3 and W4, but are poorly or undetected at the shortest wavelength, more sensitive W1 and W2 bands. Samples selected in this way are referred to as "W1W2-dropouts" by Eisenhardt et al. (2012) and Wu et al. (2012), but for brevity we use "W12drops" here as an equivalent term.

W12drop selection requires that W1 > 17.4 mag, and that either

$$\mathrm{W4} < 7.7\ \mathrm{mag} \wedge \mathrm{W2} - \mathrm{W4} > 8.2\ \mathrm{mag}, \quad (1)$$

or

$$\mathrm{W3} < 10.6\ \mathrm{mag} \wedge \mathrm{W2} - \mathrm{W3} > 5.3\ \mathrm{mag}. \quad (2)$$

Furthermore, objects are required to be farther than 30° from the Galactic Center and 10° from the Galactic Plane to limit contamination by Galactic objects. All objects are required to be free of artifacts flagged by the WISE pipeline and to not be associated with either known asteroids or those discovered by WISE (Mainzer et al. 2011).

Finally, we required candidates to pass a series of visual inspections of both individual exposures and coadded images for any given source. We focused such efforts on the brighter candidates with W4 < 7.2, resulting in a sample of 252 objects over approximately $32,000\ \mathrm{deg}^2$. We refer to these objects as the "core sample". A search to W4$\lesssim$ 7.7 using preliminary reductions covering 70% of the total area was also carried out, resulting in an additional sample of 682 W12drops which is somewhat less complete and well-characterized than the core sample. We refer to the total sample of 934 objects as the "full sample".

It is now known that WISE All-Sky profile-fitting derived fluxes of very faint sources are significantly biased due to excess sky subtraction during the data processing (see Lake et al. 2013). The effect is somewhat stochastic in nature, but can be well modeled as a constant underestimation of 9.29 ± 0.04 μJy and 10.38 ± 0.07 μJy in the W1 and W2 fluxes of the WISE All-Sky release catalog (S. Lake, private communication). Some of these issues have been corrected in the latest WISE data release, dubbed AllWISE, but because the All-Sky Catalog was used for the W12drop selection we use the WISE All-Sky fluxes and apply the corrections outlined above when modeling the selection function rather than trying to translate the W12drop selection function to the AllWISE data release. We note that the SED modeling discussed later is not affected by this issue, since we rely on deeper *Warm Spitzer* observations for those wavelengths (see §2.2.1 and §4 for details), but it will prove to be important when considering the W12drop selection function (see §5 for details).

Additionally, Wright et al. (2010) found systematic differences in the W3 and W4 magnitudes of red and blue calibrators, with the red calibrators being 17% too faint in W3 and 9% too bright in W4. Given the red col-

[13] `http://wise2.ipac.caltech.edu/docs/release/allsky/expsup/`

ors of our sources, we have corrected their W3 and W4 magnitudes by adding –0.17 mag and 0.09 mag respectively to the quantities reported in the All-Sky release for modeling their SEDs (see §3). Since these corrections are not considered by the selection criteria, we remove them when evaluating the W12drop selection function in §5. Brown et al. (2014) have recently suggested a somewhat larger correction of 0.13 mag instead 0.09 mag for sources as red as those considered here. Our main results would not be qualitatively affected by using this larger correction.

2.2. *Follow-up Observations*

2.2.1. *Warm Spitzer Observations*

We obtained observations of Hot DOGs with the IRAC instrument (Fazio et al. 2004) onboard the *Spitzer Space Telescope* (Werner et al. 2004). In its non-cryogenically cooled state, known as *Warm Spitzer*, the IRAC camera obtains photometry in two broad-band channels centered at 3.6 and 4.5μm, referred to as [3.6] and [4.5]. The channels are similar to the WISE W1 and W2 bands, but because of its larger aperture, longer exposure time, and smaller PSF (FWHM of $\approx$1.7$''$ in each band), IRAC provides significantly deeper images. We refer the reader to Griffith et al. (2012) for details of this program, as well as of the data reduction and photometric measurements.

Of the 934 W12drops in the full sample, 712 were observed with *Warm Spitzer* in the [3.6] and [4.5] IRAC channels. All but one of these is well detected in both bands, with the one outlier object (W0149–8257) detected only in the [4.5] band. We limit our parent sample to those 711 objects detected in both *Warm Spitzer*/IRAC bands. The core sample (W4<7.2) is similarly reduced to 103 targets.

2.2.2. *Ground-Based Near-IR Imaging*

We obtained follow-up near-IR observations of our sample using the Wide-field IR Camera (WIRC; Wilson et al. 2003) on the Hale 200-inch telescope at Palomar Mountain, the WIYN High-Resolution Infrared Camera (WHIRC; Meixner et al. 2010) at the 3.5m WIYN telescope, the Ohio State InfraRed Imager/Spectrometer (OSIRIS; Depoy et al. 1993) at the 4m SOAR telescope, and the SAO Widefield InfraRed Camera (SWIRC; Brown et al. 2008) at the 6.5m MMT telescope. Table 2 provides more details about these observations.

All images were reduced following standard IRAF procedures using the XDIMSUM package[14], and all fluxes were obtained in 4.0$''$ diameter apertures. Each image was flux-calibrated using the 2MASS point source catalog (PSC, Skrutskie et al. 2006), using comparison stars within the field of view whenever possible, or by using the closest observation in time of a field containing 2MASS detected stars if conditions were photometric. The latter was only necessary for some of the OSIRIS observations, which have an 80$''$ field of view. We add the dispersion of the zero-point calibration in quadrature to the photometric uncertainty of each source. Magnitudes are listed in Table 2 for each of the W12drops for which we obtained follow-up near-IR observations.

[14] `ftp://iraf.noao.edu/ftp/extern-v214/xdimsum`

Table 2
Ground-Based NIR Follow-Up

WISE ID	Band	Mag†	Unc.	Instrument‡
WISEJ000431.34–192301.8	H	19.453	0.125	A
WISEJ000709.03+730831.2	J	21.795	0.630	B
WISEJ002659.24+201556.2	J	20.270	0.117	B
	Ks	18.833	0.142	C
WISEJ002933.06+020505.4	J	19.794	0.166	B
WISEJ012611.98–052909.6	J	19.861	0.135	B
WISEJ013400.59–260726.5	J	20.163	0.123	A
WISEJ014747.59–092350.5	J	>23.000		B

Note. — Table 2 is published in its entirety in the electronic edition of ApJ. A portion is shown here for guidance regarding its form and content.
† 1σ upper bounds shown for undetected sources.
‡ Telescope and instrument used for the observations, defined as **A**: SOAR/OSIRIS; **B**: WIYN 3m/WHIRC; **C**: Hale 200-inch/WIRC; and **D**: MMT/SWIRC.

Of the 711 (103) objects in our full (core) W12drop sample with *Warm Spitzer* observations, 84 (52) have been observed in J-band, 23 (16) in H-band, and 37 (19) in K-band. Of these, only 1 (0) object has been observed in all three bands, and only 26 (16) have been observed in more than one band.

2.2.3. *Optical Spectroscopy*

Optical spectroscopy was performed for a large fraction of our sample using several facilities, with greater emphasis given to the core sample. These were obtained primarily using LRIS on the Keck-I telescope (see Wu et al. 2012, for examples) and GMOS-S on the Gemini-S telescope. Redshifts are generally based on multiple features and are therefore considered secure. Eisenhardt et al. (in prep.) will provide a comprehensive description of the optical spectroscopy. Figure 1 shows the redshift distribution of all 115 (58) objects in the full (core) W12drop sample with *Warm Spitzer* observations and successful redshift measurements. The full sample shows a clear minimum at $0.6 < z < 2$, suggesting the low- and high-redshift populations are distinct. The core sample distribution is also consistent with the presence of the bimodality, albeit at lower significance due to the smaller number of objects. Since we are only interested in very luminous objects, we focus on the sample of 96 (52) objects from the full (core) sample with $z > 1$. Eisenhardt et al. (in prep.) shows that approximately 70% of the objects targeted for spectroscopy yielded redshift measurements, but that objects with failed spectroscopic measurements are primarily due to optical faintness, suggesting they are typically located at high redshift and are bona-fide HyLIRGs. We note that during some of the spectroscopic observing runs, we biased against targets detected in both the B and R bands of the Digitized Sky Survey[15] to reduce the incidence of low redshift contaminants. This bias has only a minor effect for the $z > 1$ population, so we do not discuss it any further.

3. SED MODELING METHODOLOGY

[15] `https://archive.stsci.edu/cgi-bin/dss_form`

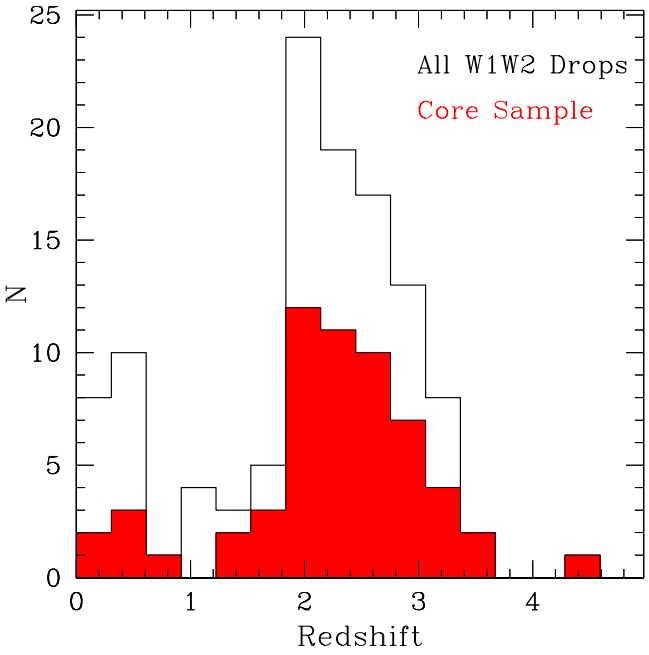

Figure 1. Redshift distribution of the 115 W12drops with spectroscopic redshift and IRAC measurements. The shaded histogram shows the distribution for the 58 objects in the core sample (W4<7.2, see §2.1).

In order to gain insight into the physical properties of Hot DOGs, we study their rest-frame optical through mid-IR multi-wavelength SEDs. Specifically, we study their rest-frame optical through mid-IR properties by combining the WISE data with optical spectroscopy, *Warm Spitzer* observations and ground-based near-IR photometry. We model the SEDs following the approach applied in Eisenhardt et al. (2012) to study Hot DOG W1814+3412. Namely, we use the low resolution AGN and galaxy SED templates and the respective modeling algorithm of Assef et al. (2010). Briefly, every object is modeled as a non-negative linear combination of three host galaxy SED templates (broadly resembling E, Sbc and Im types, see Assef et al. 2010, for details) and one AGN SED template. Eisenhardt et al. (2012) used the AGN template of Richards et al. (2006) because of its longer wavelength range. Here we use the Assef et al. (2010) AGN template instead, but there is no substantial difference between these AGN templates for the purpose of the SED modeling of Hot DOGs over the UV-through-mid-IR wavelength range studied in this work.

We also fit an AGN reddening component, which we parametrize by the color excess $E(B-V)$, considering values from 0 to $10^{1.5}$. The assumed reddening-law corresponds to an SMC-like extinction for $\lambda < 3300$Å, and a Galactic extinction curve at longer wavelengths. Additional details are provided in Assef et al. (2010). Although in some unresolved obscured sources it may be important to modify these reddening curves to account for the optical and UV photons scattered into the line-of-sight (see Kochanek et al. 2012), our sources are under too much obscuration for this to be a significant issue. In the next sections we show that this approach does, in general, perform a good job of modeling Hot DOGs, although possible shortcomings are discussed in detail.

One of the important quantities we want to study is the intrinsic bolometric luminosity of the underlying AGN. We estimate it using the scaling relation of Kaspi et al. (2000),

$$L_{\rm AGN}^{\rm Bol} \;=\; 9\;\lambda L_{\lambda}(5100\text{Å}). \qquad (3)$$

The continuum luminosity at 5100Å is calculated by taking only the best-fit reddened AGN component, and removing the obscuration. While a more self-consistent bolometric luminosity can be obtained by integrating over the best-fit AGN component to the SED (see, e.g., Assef et al. 2010, 2013; Eisenhardt et al. 2012), this scaling is widely used, so adopting it simplifies the comparison with other results in the literature. For reference, the luminosity obtained integrating over the unreddened AGN template between 0.1 and 30μm is greater than the bolometric luminosity estimated using equation (3) by a factor of 1.3. By using a single AGN template we are implicitly assuming the torus covering fraction of the accretion disk in all Hot DOGs is equal to that implied by the template, which is likely about 50% given the results of Assef et al. (2013). For luminous Type 1 quasars Roseboom et al. (2013) found that the mean covering fraction was 39% with a dispersion of 18%. Since the amplitude of the AGN component in the best-fit SED is primarily anchored by the W3 and W4 fluxes, a larger covering fraction could reduce the deduced AGN continuum luminosity at 5100Å. In principle, this luminosity could be overestimated by up to a factor of 2 in the extreme scenario where the torus leaves no open line of sight towards the accretion disk and is composed of uniformly distributed hot dust clouds, as all dust must strongly radiate at $\lambda \lesssim 10\mu$m to affect our results. This scenario is, however, unlikely, given the detection of AGN narrow-emission lines in many of the rest-frame UV spectra (see, e.g. Wu et al. 2012).

We also wish to estimate the stellar mass (M_*) of each host galaxy. We estimate this quantity by multiplying the rest-frame luminosity of the host component in the K-band by the mass-to-light ratio (M/L) in that band. The value of M/L depends on many parameters, including the galaxy's star-formation history, metallicity, stellar initial mass function (IMF) and contribution from thermally pulsating asymptotic giant branch (TP-AGB) stars. Because we generally have only a single photometric band probing the host properties, we only aim to place meaningful bounds on M/L. Although the lower end of the M/L range is only loosely bound, the upper end is much better constrained, as it is primarily limited by the age of the Universe at the redshift of the object. Hence, for the purpose of this study, we will focus on estimating upper bounds on the stellar mass of each Hot DOG. We estimate these upper bounds for each object using the EzGal code of Mancone & Gonzalez (2012) with the stellar population models of Bruzual & Charlot (2003). We choose these stellar population models in favor of more recent ones available for EzGal (e.g., Maraston 2005; Conroy et al. 2009; Conroy & Gunn 2010) since they have the lowest contribution of TP-AGB stars to the composite SEDs, implying the highest M/L values. The M/L values in the rest-frame near-IR are rather insensitive to variations in the metallicity, with lower metallicities implying higher M/L values in K_s. To be

conservative we consider the lowest metallicity available for EzGal, $Z = 0.008$ ($\equiv 0.4 Z_{\odot}$). For the star-formation history, we consider a simple stellar population (SSP) with a formation redshift $z_F = 15$. Finally, for the IMF, we consider the results of Conroy et al. (2013), who have shown that in early-type galaxies, the M/L ratio in K-band can be up to twice that expected for the Milky Way. We use M/L values two times higher than those estimated assuming a Chabrier (2003) IMF. Our only assumption that would tend to underestimate the stellar mass is that of little host obscuration in the rest-frame K-band. We discuss this issue further in detail in §4 and §6, where evidence is shown that although Hot DOGs live in significantly dense regions, possibly clusters or dense filaments, higher stellar masses would predict even richer environments than observed.

Finally, we also attempt to estimate the central SMBH mass ($M_{\rm BH}$) for these objects. In many cases, however, we do not quote the values of $M_{\rm BH}$ but of the Eddington luminosity defined as

$$L_{\rm Edd} \; = \; 3.28 \times 10^4 \; \left(\frac{M_{\rm BH}}{M_{\odot}} \right) \; L_{\odot}, \qquad (4)$$

which corresponds to the luminosity at which photon pressure inhibits isotropic accretion onto an isotropically radiating body. This is an interesting quantity to study for AGN since most energy is generated by accretion onto the SMBH. Furthermore, Kollmeier et al. (2006, also see Shen et al. 2008) have shown that luminous QSOs at similar redshifts as Hot DOGs tend to radiate in a limited range of Eddington ratios, defined as $\lambda_E = L^{\rm Bol}_{\rm AGN}/L_{\rm Edd}$.

Direct estimates of $M_{\rm BH}$ in AGN, and hence $L_{\rm Edd}$, based on single optical spectra are possible by combining the width of their broad emission lines and the luminosity of their accretion disks (e.g., Vestergaard & Peterson 2006), typically limiting such measurements to unobscured objects. In an upcoming article (Wu et al. in prep.) we explore such estimates for a handful of Hot DOGs where we observed broad Hα in the near-IR, but such methods are certainly not applicable to the sample of objects we study here. Hence, we consider two alternative methods, and explore their consequences in depth in §4. First, we estimate $M_{\rm BH}$ through equation (4) by assuming that the AGN in Hot DOGs radiate at the typical $\lambda_E = 0.30$ determined by Kollmeier et al. (2006) for QSOs at similar redshifts. Alternatively, we assume that $M_{\rm BH}$ is related to the stellar mass in the host galaxy in the same way as found for local galaxies. Specifically, we use the relation between the spheroidal component mass ($M_{\rm Sph}$) and $M_{\rm BH}$ of Bennert et al. (2011a),

$$\log \frac{M_{\rm BH}}{M_{\odot}} \; = \; -3.34 \; + \; 1.09 \log \frac{M_{\rm Sph}}{M_{\odot}}. \qquad (5)$$

Given that the near-IR imaging reported here is either ground based or from *Spitzer*, we cannot attempt a morphological decomposition of the bulge or spheroidal component. Furthermore, due to the extreme nature of Hot DOGs, it is not even clear the definition of a spheroidal component would be sensible. Hence, we assume that all of the detected rest-frame K-band light belongs to the spheroidal component. Combined with the fact that our stellar mass estimates are also upper bounds, our estimates of $M_{\rm BH}$ obtained in this manner should be considered as generous upper limits. In the next section we discuss how both estimates lead to very different scenarios for Hot DOGs, highlighting that accurate estimates of $M_{\rm BH}$ in Hot DOGs are a crucial element for understanding their nature, requiring more extensive optical/near-IR spectral coverage.

Due to the low number of degrees of freedom, there can be considerable uncertainty for the best-fit parameters of each galaxy. To account for this, we do a Monte Carlo approach. For each object we resample each available flux from a Gaussian distribution centered at the measured value with a standard deviation equal to the photometric uncertainty, and re-estimate all the parameters described above. We repeat this 1000 times per galaxy and re-estimate the results discussed in the next section, finding no significant difference.

Finally, we caution that the infrared emission might not be powered by AGN activity but might be powered by extreme starburst disks, such as proposed by Thompson et al. (2005), who found that, under the appropriate conditions, a disk of star-formation can form where gas and dust are supported primarily by star-formation feedback and radiation pressure. The typical dust temperature can become quite high, comparable to the temperatures of $\sim$ 60 K typical of Hot DOGs (Wu et al. 2012). Extreme star-formation rates, on the order of $\sim 10^4$ M$_{\odot}$ yr^{-1}, would be needed to power the luminosities seen in Hot DOGs (see, e.g. Eisenhardt et al. 2012), making this scenario quite unlikely. Also, Thompson et al. (2005) find that it is inevitable to form a bright AGN at the center of such a starburst disk and that, furthermore, the star-formation driven rest-frame 10μm emission still relates to the accretion disk emission in the same way as for a regular Type 1 QSO as judging from the templates of Elvis et al. (1994). Hence, even in this arguably unlikely physical scenario, the main results presented here are still valid. We do not refer to this scenario hereafter.

4. ANALYSIS

By design, W12drops are either undetected or marginally detected in W1 and W2. Because of this, we fit their SEDs using the *Warm Spitzer* [3.6] and [4.5] photometry, W3 and W4 photometry, and, whenever possible, the ground-based near-IR photometry. Figure 2 shows examples of SED fits to two high-redshift and two low-redshift W12drops. Objects with $z < 1$ have much lower luminosities and are much worse fit by the models than their higher-redshift counterparts, reinforcing the idea they compose two distinct populations. From now on, we will use interchangeably the terms "Hot DOG" (Wu et al. 2012) and "W12drop at $z > 1$" for convenience in this article.

Our SED fits show that the AGN component dominates the luminosity of Hot DOGs, accounting for >97% of the total $0.1 - 30\mu$m output in all objects. Figure 3 shows the residuals of the SED fits both as a ratio between the observed and model fluxes (top panel) and as the difference with respect to the measurement uncertainties (bottom panel). The ground-based near-IR photometry shows large discrepancies with respect to the modeled fluxes but only in absolute terms, as the deviations are in almost no case beyond 3σ. The *Warm Spitzer*/IRAC and W3-4 fluxes show only small abso-

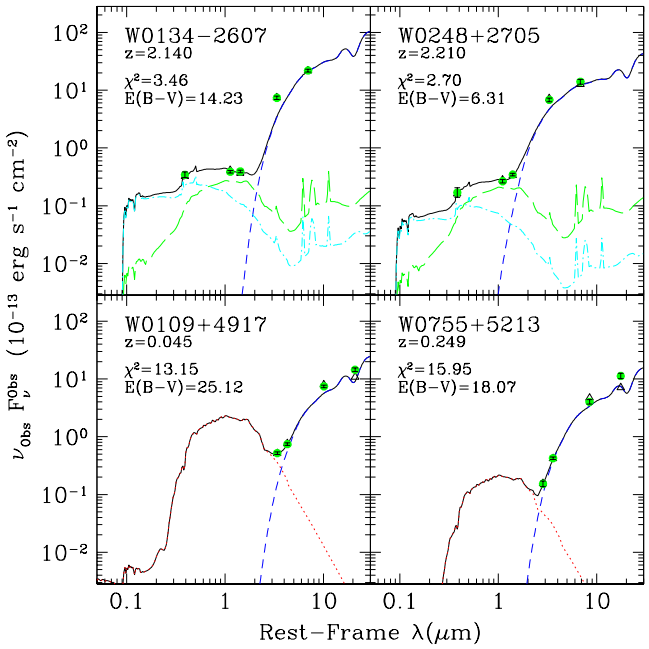

Figure 2. Examples of SED fits to two high-redshift (top panels) and two low-redshift W12drops (bottom panels). All four have χ^2 values close to the median values of their populations. Each panel shows the observed fluxes (*green filled circles*), as well as the expected fluxes from the best-fit SED model (*black open triangles*). The solid lack line shows the best-fit SED, composed of an AGN under $E(B-V)$ of obscuration (*dashed blue line*) plus a quiescent (*dotted red*), intermediate (*long-dashed green line*) and strongly star-forming (*dot-dashed cyan line*) stellar populations (see §3 for details). Most galaxies do not require all three stellar templates. Notice the much higher χ^2 values of the low-redshift galaxy fits.

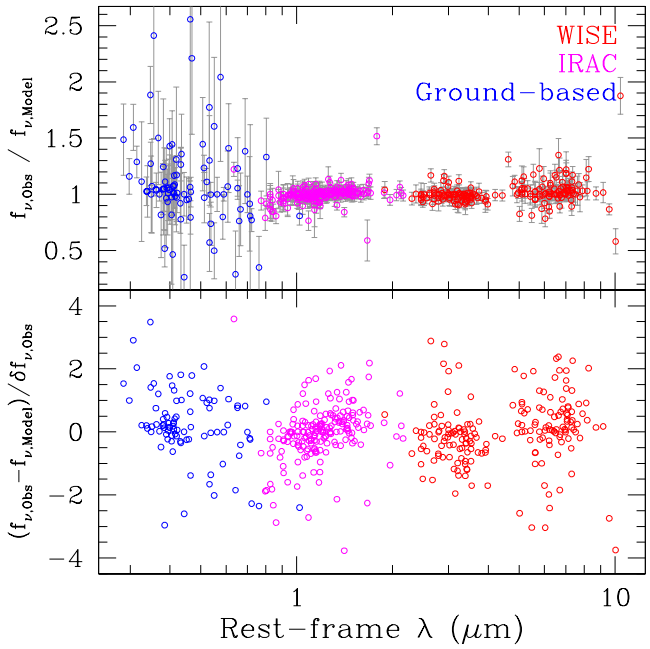

Figure 3. Flux residuals of the SED models for the 89 out 96 Hot DOGs with $\chi^2 < 20$.

lute discrepancies from the model, without a significant systematic component. The lack of systematic residuals also suggests it is unlikely there is a significant amount of unrecognized obscuration on the host galaxy that would bias our maximal stellar mass estimates (see §3).

Figure 4 shows the distribution of the bolometric luminosity of the AGN component $L^{\rm Bol}_{\rm AGN}$ for Hot DOGs in the full sample as well as in the core sample. Hot DOGs tend to have quite luminous AGN, with bolometric luminosities between 10^{47} and 10^{48} erg s^{-1}. In the same panel, we show the values of the characteristic quasar luminosity function (QLF) luminosity L^* at two different redshifts, $z = 1.0$ and 2.0, determined by converting appropriately the values of $M_{*,J}$ determined by Assef et al. (2011). The AGN components in Hot DOGs are among the most luminous AGN at their redshifts. We discuss this further in §5.

Figure 5 shows the distribution of dust obscuration towards the accretion disk, parametrized by $E(B-V)$. Eisenhardt et al. (2012) studied Hot DOG W1814+3412 in detail using 8 bands of optical through mid-IR photometry, finding an obscuration of $E(B-V) = 15.6 \pm 1.4$ with a very similar approach to that used here. With an updated processing of the WISE data and the corrections to W3 and W4 discussed in §2.1 but a more limited multi-wavelength photometry set than that used by Eisenhardt et al. (2012), we find here a lower obscuration of $E(B-V) = 11.7 \pm 1.2$ for W1814+3412. This obscuration is lower primarily due to the W3 and W4

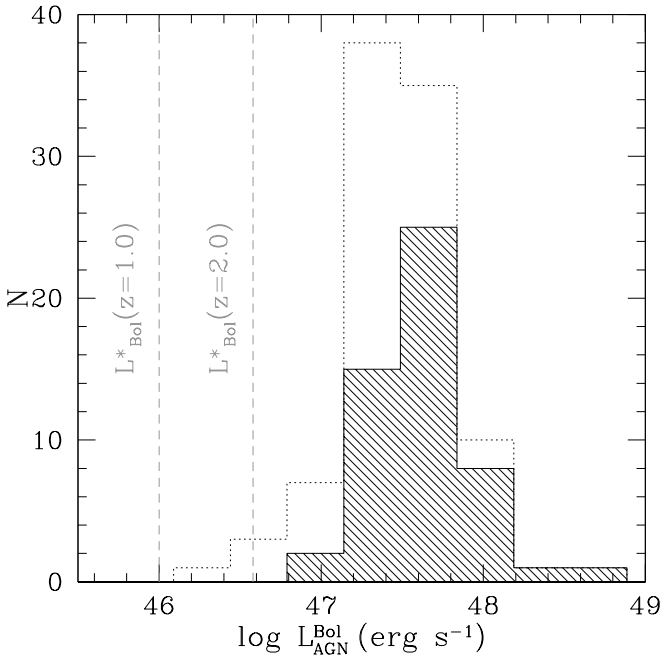

Figure 4. Distribution of AGN bolometric luminosities derived from our SED modeling of Hot DOGs (see §3 and §4 for details). The solid hashed histogram shows the distribution of the core sample (i.e., W4<7.2), while the dashed open one shows the distribution of the full sample. The vertical dashed gray lines show the characteristic AGN bolometric luminosity derived from the J-band QLF of Assef et al. (2011), assuming the unobscured AGN SED template of Assef et al. (2010) and equation (3).

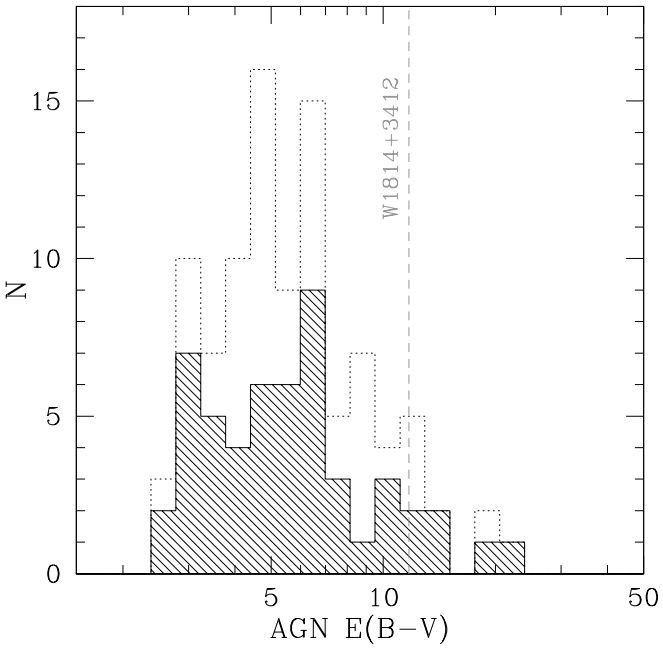

Figure 5. Distribution of AGN obscurations derived from our SED modeling of Hot DOGs (see §3 and §4 for details). The solid hashed histogram shows the distribution of the core sample (i.e., W4<7.2), while the dashed open one shows the distribution of the whole sample. The dashed gray line shows the obscuration derived for HyLIRG W1814+3412, studied by Eisenhardt et al. (2012). For reference, we note that for the reddening law used in this article, the attenuation factor at 1μm is given by $A_{1\mu m} = 1.24 * E(B-V)$.

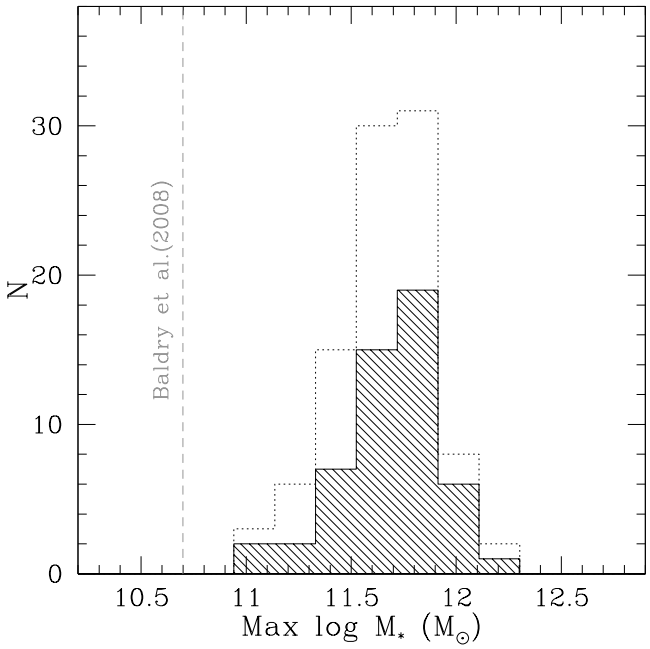

Figure 6. Distribution of stellar mass upper bounds derived from our SED modeling of Hot DOGs (see §3 and §4 for details). The solid hashed histogram shows the distribution of the core sample (i.e., W4<7.2), while the dashed open one shows the distribution of the whole sample. The dashed gray line shows the stellar mass of an $L*$ galaxy today from Baldry et al. (2008).

band corrections applied here. If we do not consider these corrections, we find an obscuration of $E(B-V) = 15.1 \pm 1.2$ for W1814+3412, consistent with the value found by Eisenhardt et al. (2012). Figure 5 shows that W1814+3412 has significantly more obscuration than the average Hot DOG, for which $\langle E(B-V)\rangle = 6.8$ in the core sample and $\langle E(B-V)\rangle = 6.4$ in the full sample. For completeness, we note the median obscuration is $E(B-V) = 6.0$ in the core sample and $E(B-V) = 5.5$ in the full sample. The best-fit AGN obscuration for Hot DOGs ranges between $2.5 < E(B-V) < 21.5$. Assuming the median gas-to-dust ratio of Maiolino et al. (2001), $E(B-V)/N_{\rm H} = 1.5 \times 10^{-23}$ cm^2 mag, the average obscuration corresponds to gas column densities of approximately of 4×10^{23} cm^{-2}, and a range of $1.6 \times 10^{23} < N_{\rm H} < 1.4 \times 10^{24}$ cm^{-2}. This is over 10 times more absorption than the typical dividing line between Type 1 and Type 2 AGN ($N_{\rm H} = 10^{22}$ cm^{-2}; see, e.g., Ueda et al. 2003), to just being slightly below Compton thick ($N_H > 1.5 \times 10^{24}$ cm^{-2}). Using X-ray observations of a sample of three Hot DOGS obtained with *XMM-Newton* and *NuSTAR*, Stern et al. (2014) inferred for each of them neutral hydrogen column densities of $N_{\rm H} \gtrsim 10^{24}$ cm^{-2}, consistent with Compton-thick obscuration, and in good agreement with the values inferred above from dust obscuration.

Figure 6 shows our maximal stellar mass estimates. For reference, we also show the stellar mass of an $L*$ galaxy today ($\sim 5 \times 10^{10}$ M$_\odot$; e.g., Baldry et al. 2008). Even if we were to assume a mass-to-light ratio 10 times lower, as appropriate for extreme starbursts, Hot DOGs would still have massive host galaxies. In §6 we further discuss these host mass estimates and explore their environments in the context of such massive host galaxies. However, as massive as the host galaxies are, the AGN still dominates the emission by orders of magnitude, which has very interesting implications for the nature of Hot DOGs depending on the mass of their SMBH. As discussed earlier, however, we are not able to obtain unique estimates of $M_{\rm BH}$. Below we explore two scenarios for which we can estimate $M_{\rm BH}$ based on indirect considerations as well as the implications of each scenario to the nature of Hot DOGs.

4.1. $M_{\rm BH}$ *Estimates based on a Fixed* λ_E

The first scenario estimates $M_{\rm BH}$ assuming a fixed Eddington ratio of $\lambda_E = 0.30$, the same Eddington ratio as that determined by Kollmeier et al. (2006) for $z \sim 2$ QSOs. Since the AGN emission is so luminous, a very large $M_{\rm BH}$ is needed to have an SMBH accreting at the same level of regular QSOs. In fact, the SMBH mass is much larger than expected for the local stellar bulge to $M_{\rm BH}$ ratio (Bennert et al. 2011a) and the stellar mass of the host galaxy, even for the upper limits calculated above, as shown in Figure 7. Even if we assume that the stellar mass is equal to the upper bound and is dominated by an spheroidal component, Hot DOGs sit an order of magnitude above the local relation, but the discrepancy is likely much larger. If these galaxies are to evolve in such a way that at $z = 0$ they would fall in the local measured relations, the bulge will have to grow at a much faster rate than the accreting central SMBH, implying that SMBH growth precedes the host galaxy growth. In such a scenario, the stellar mass growth could

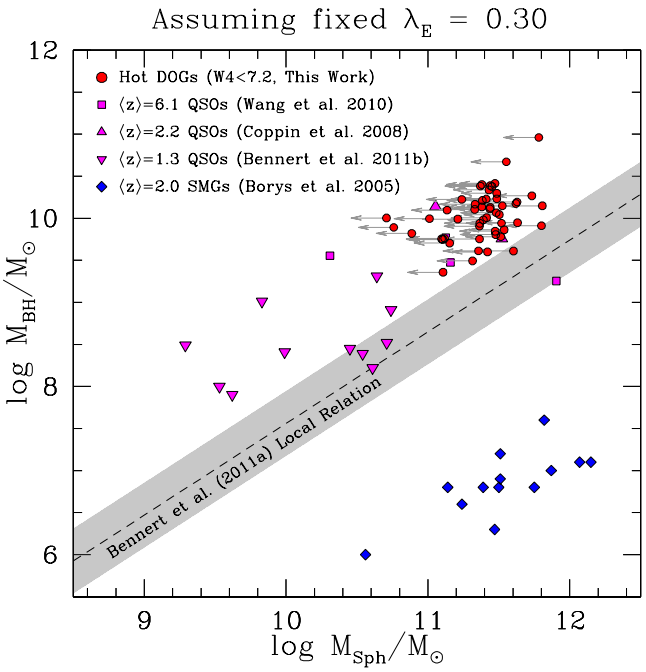

Figure 7. The position in the $M_{\rm BH}-M_{\rm Sph}$ diagram of Hot DOGs (*red circles*) if we assume the AGN in Hot DOGs radiate at the typical $\lambda_E = 0.30$ of $z \sim 2$ QSOs. For comparison, we also show the relation of local active galaxies determined by Bennert et al. (2011a), as well as the position in the diagram of different high redshift populations in the literature, as described in the top left labels. For the literature samples, the label shows their respective mean redshifts.

not be quenched by intense AGN activity, as is assumed in many evolution models of massive galaxies (as in, e.g., Hopkins et al. 2008), since the epoch of intense SMBH growth significantly precedes the end of the host galaxy assembly, but may be consistent with quenching by low-level AGN accretion through radio-mode feedback (as in, e.g., Croton et al. 2006).

While this discrepancy can be alleviated by considering a larger value for λ_E, it is consistent with what has been found previously for some Type 1 QSOs. For example, Bennert et al. (2011b) studied the evolution of the $M_{\rm BH}-M_{\rm Sph}$ relation with cosmic time using a sample of $z \sim 1$ unobscured QSOs observed with the *Hubble Space Telescope* where $M_{\rm Sph}$ was determined through SED and morphological modeling of the host. Bennert et al. (2011b) found a trend in the same direction suggested by our data, namely $M_{\rm BH}/M_{\rm Sph} \propto (1+z)^{1.96\pm0.55}$, while combination with more heterogeneous measurements in the literature yielded $M_{\rm BH}/M_{\rm Sph} \propto (1+z)^{1.16\pm0.15}$. Figure 7 shows the set of objects studied in detail by Bennert et al. (2011b), illustrating a displacement from the local relation comparable to that of Hot DOGs. Similar results have also been obtained for unobscured QSOs at $z \sim 6$ by Wang et al. (2010, and references therein) and at $z \sim 2$ by Coppin et al. (2008), where the host stellar masses come from dynamical estimates based on CO emission and the assumption of random orientation (i.e., $i = 32.7^o$). These findings support the assumption that the AGN in Hot DOGs radiate at the same λ_E as similar redshift QSOs. For comparison, Figure 7 also shows the location in this diagram of $z \sim 2$ SMGs, as determined by Borys et al. (2005), which are highly discrepant from the local relation but in the opposite direction to QSOs. Interestingly, Bongiorno et al. (2014) has recently shown that $z \sim 2$ Type 1.8/1.9 QSOs may actually show better agreement with the local relation than Type 1 QSOs, with a discrepancy that may depend on $M_{\rm BH}$.

A different picture to interpret these results is that proposed by Peng (2007, see also Jahnke & Macciò 2011), who have argued that the local host galaxy - black hole mass correlations can naturally arise through galaxy mergers without co-evolution between them and no initial relation. The prediction for that scenario is that the dispersion of the $M_{\rm BH}-L_{\rm Bulge}$ relation would increase substantially with redshift, possibly consistent with the large spread observed in Figure 7. Hot DOGs and QSOs could then be regarded as the tail of that distribution, namely exceedingly massive black holes in faint host galaxies.

4.2. $M_{\rm BH}$ *Estimates based on the Local* $M_{\rm BH}-M_{\rm Sph}$ *Relation*

In the second scenario, we assume that the local relationship between the spheroidal component stellar mass and $M_{\rm BH}$ is appropriate for Hot DOGs (see §3), and obtain an upper bound of the SMBH mass from the estimates of the maximal stellar mass. Combined with the AGN bolometric luminosity of Hot DOGs, this provides an estimate of the "minimum" Eddington ratio (λ_E) at which the AGN is radiating. Figure 8 shows the distribution of the implied Eddington ratio of Hot DOGs. The peak is about 2–3 times the Eddington limit, and almost all objects are accreting at $\lambda_E \geq 1$. For comparison, we show the typical Eddington ratio of ~ 0.30 for QSOs at a redshift of ~ 2 determined by Kollmeier et al. (2006).

Although the scenario discussed in §4.1 may seem more likely, Hot DOGs might indeed be radiating at several times their Eddington limit. Note the Eddington limit is not necessarily a hard, physical boundary in this case, since the accretion is most likely not isotropic. Due to photon pressure, it is possible that the AGN would be in the process of mechanically expelling material from the regions close to the central SMBH and, possibly, from the galaxy's potential well. This would be consistent with the high fraction of extended Lyα emission reported by Bridge et al. (2013), and may relate specifically to the key stage in the standard galaxy evolution paradigm where star-formation is being shut down, and thus transitioning to the QSO stage where it will remain until the accreting gas supply stops (see, e.g., Hopkins et al. 2008). Were we to assume the evolving $M_{\rm BH}/M_{\rm Sph}$ relation of Bennert et al. (2011b, see §4.1), our SMBH masses would be underestimated by a factor of 3.5–5 and the AGN in the Hot DOG population would still be radiating at, or close to the Eddington limit, well above the mean QSO Eddington ratio found by Kollmeier et al. (2006, see Fig. 8). A correction factor closer to 10 is needed to yield consistency with the mean λ_E of Kollmeier et al. (2006). In §5 we discuss the number density of these objects and further argue that Hot DOGs might indeed be radiating at high Eddington ratios.

The presence of extended Lyα emission may put interesting constraints on the lifetime of Hot DOGs if we assume it comes from winds launched by a super-Eddington

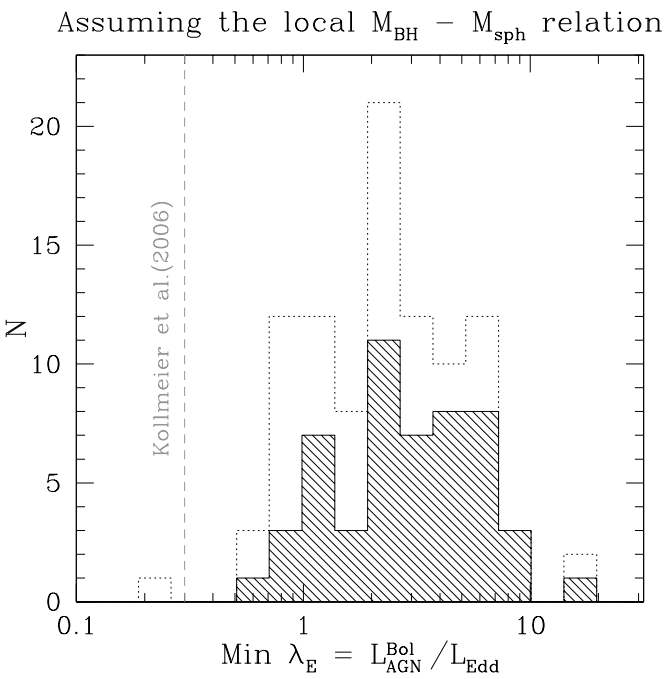

Figure 8. Distribution of the minimum Eddington ratio for the AGN in Hot DOGs, assuming that the local relation between $M_{\rm Bulge}$ and $M_{\rm BH}$ holds at high redshift. The solid hashed histogram shows the distribution of the core sample (i.e., W4<7.2), while the dashed open one shows the distribution of the whole sample. The dashed gray line shows the the peak Eddington ratio found by Kollmeier et al. (2006) for $z \sim 2$ Type 1 QSOs.

accreting AGN. Bridge et al. (2013) find the emitting gas has projected velocities of up to several thousand km s^{-1}. Assuming a constant velocity of $\sim 10,000$ km s^{-1}, for the gas to have been launched from the central regions of the galaxy, this stage would have to last $\gtrsim 10$ Myr to reach a distance of ~ 100 kpc. This is consistent with the lifetimes of 1 Myr $<$ t$_{\rm QSO}$ $<$ 20 Myr estimated by Trainor & Steidel (2013) for a sample of hyper-luminous QSOs (which they defined as $L_{\rm UV} \sim 10^{14}\ L_\odot$). On the other hand, if the gas were simply responding to the emission of the AGN but was not associated to feedback, the light travel time puts a weak constraint on the lifetime of this phase to $\gtrsim 3 \times 10^5$ yr.

5. NUMBER DENSITIES OF HOT DOGS AND QSOS

Several lines of evidence imply that Hot DOGs are indeed powered by heavily obscured AGN (Wu et al. 2012; Eisenhardt et al. 2012, in prep.), and so it is natural to compare their properties to those of comparably luminous but unobscured Type 1 QSOs, which are much better studied. The simplest comparison is of their space densities. For this, we focus on the core sample of 252 W12drops described in §2.1 (i.e., W4<7.2). We know that of the 103 core W12drops with *Warm Spitzer*/IRAC observations, 58 have reliable spectroscopic redshifts. Of these, 52 (90%) are at $z \geq 1$ and can hence be considered Hot DOGs, while 43 (74%) are at $z \geq 2$. Assuming that objects without spectroscopic redshift measurements have a redshift distribution approximately equal to that of the spectroscopic sample (Eisenhardt et al. in prep.), there are 187 Hot DOGs with $z \geq 2$ and W4<7.2. Of them, Hot DOG W2246–0526 ($z = 4.6$) is the only one at $z > 4$ and it seems to be somewhat of an outlier based on its photometric properties, so we will limit the study to the Hot DOGs in the redshift range $2 < z < 4$.

We study the effects of the selection function using the 42 core sample Hot DOGs with reliable spectroscopic redshifts in the range $2 < z < 4$ and IRAC observations. Because the Hot DOG selection is based upon the observed WISE magnitudes and colors, objects identified as core sample Hot DOGs may not have been recognized as such if located at a different redshift. This causes a significant sample incompleteness which we take into account by using the $V/V_{\rm Max}$ method of Schmidt (1968). In short, we use the best-fit SED model of each individual source to evaluate the redshift range, and hence volume V, for which the object could have been detected and identified by WISE as a Hot DOG within the full volume $V_{\rm Max}$, corresponding to the redshift range $2 < z < 4$. We then simply assume that the intrinsic distribution of sources is uniform across the given volume $V_{\rm Max}$ such that the effective number surface density of Hot DOGs is then

$$N_{\rm HD} \ = \ \frac{1}{f_z A_{\rm Sky}} \ \sum_i \ \frac{1}{V_i/V_{\rm Max}}, \qquad (6)$$

where $f_z = 58/252 = 0.23$ is the fraction of core sample Hot Dogs with IRAC observations and a reliable redshift measurement, and $A_{\rm Sky} = 32,000$ deg^2 is the area of the sky surveyed for Hot DOGs. We estimate the error as

$$\delta N_{\rm HD} \ = \ \frac{1}{f_z A_{\rm Sky}} \ \left(\sum_i \ \frac{1}{(V_i/V_{\rm Max})^2} \right)^{1/2} . \qquad (7)$$

Two caveats to this process should be noted. First, we apply the corrections of Lake et al. (2013, and Lake, S. private comm.) to the model fluxes before evaluating the selection function to account for the flux bias of the WISE All-Sky release (see §2.1 for details). And, second, we apply a small correction to the W3 and W4 model fluxes to perfectly match the observed values at the object's redshift. Even after applying the flux bias correction, we find that 10 of the 52 Hot DOGs in the core sample with IRAC observations and spectroscopic $z \geq 1$ (6 of which are in the redshift range $2 < z < 4$) were only selected as such because of the stochastic nature of the flux bias. The SED modeling of these objects, driven primarily by the IRAC fluxes, predicts W1 and W2 fluxes too bright to be selected as Hot DOGs. We do not use these objects to estimate $N_{\rm HD}$. Note the change to f_z from eliminating these 7 objects from the sample is negligible, decreasing from 0.23 to 0.21.

Using equation (6) we find then that the effective number surface density of Hot DOGs is $N_{\rm HD} = 0.032 \pm 0.004$ deg^{-2}, or approximately one for every 31 ± 4 deg^2. Figure 9 shows the cumulative, volume-corrected surface density of Hot DOGs as a function of increasing luminosity of the obscured AGN component. We parametrize the AGN component luminosity by $M_J^{\rm AGN}$, the absolute J-band magnitude it would have under no obscuration. A drawback of our $V/V_{\rm Max}$ approach to correct for incompleteness is that it disregards evolution in the Hot DOG number density between $2 < z < 4$. Furthermore, using such a large redshift range can lead to very large correction factors, which could be introducing significant noise

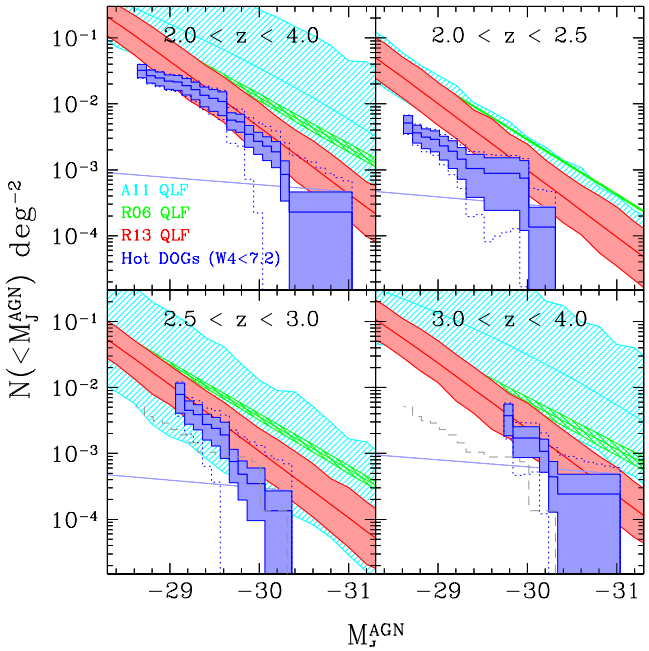

Figure 9. The top left panel shows the number density of Hot DOGs in the redshift range $2 < z < 4$ (*solid blue line*) corrected for volume incompleteness through the $V/V_{\rm Max}$ approach of Schmidt (1968, see §5 for details). We also show the region marked by the error-bars (*solid blue region*). The dotted blue lines show the uncertainty region taking into account a nominal scatter in the AGN covering fractions, as discussed in the text. For comparison, we also show the expected number density of Type 1 QSOs as predicted by the QLFs of Richards et al. (2006, *green*), Assef et al. (2011, *cyan*) and Ross et al. (2013, *red*). The remaining three panels show the same but for three redshift slices within the full range. For comparison, the Hot DOG distribution of the $2 < z < 2.5$ slice is shown in the other two slices (*dashed gray line*).

to our estimates. To avoid these issues, Figure 9 also shows the effective number of Hot DOGs as a function of the AGN component luminosity for three redshift slices: $2 < z < 2.5$, $2.5 < z < 3$ and $3 < z < 4$. Due to the low number of sources, the uncertainties are large in the last redshift bin. Interestingly, little evolution is observed between the first two redshifts slices, while some evolution may be present when compared to the $3 < z < 4$ slice. The statistics are currently insufficient to be more definitive about this.

The estimates of $M_J^{\rm AGN}$ from our SED modeling are based on the assumption of a single AGN covering fraction (c_f) for all Hot DOGs, as discussed in §3. It is possible, however, that there is a significant scatter on the c_f of Hot DOGs. To explore this we re-estimate the uncertainty regions now including the effects of a scatter in c_f equal to that found by Roseboom et al. (2013) for Type 1 QSOs. The scatter in c_f found by Roseboom et al. (2013) can be expressed as an uncertainty of 0.5 mag in the magnitude of any band dominated by the accretion disk emission for a fixed mid-IR flux. Although the rest-frame J-band luminosity is only partly powered by the accretion disk, we consider the full 0.5 mag uncertainty in our estimates of $M_J^{\rm AGN}$ for simplicity. Figure 9 shows the uncertainty region considering the effects of such a scatter. Including this effect increases the size of the uncertainty region, particularly at the bright end, but does not qualitatively change our results.

To obtain the number density of comparably luminous Type 1 AGN we use the functional form of the optically selected QLF of Richards et al. (2006) and Ross et al. (2013), derived from SDSS observations, and of the mid-IR and X-ray selected QLF of Assef et al. (2011), derived from the deeper but smaller area observations of the NDWFS Boötes field. The brighter end of the luminosity function is much better constrained by the SDSS observations used by Richards et al. (2006) and Ross et al. (2013) than by the much smaller Boötes field used by Assef et al. (2011), suggesting they are a better comparison to our HyLIRG sample. However, the mid-IR nature of our Hot DOG selection may be better represented by the selection function of Assef et al. (2011). We note that Richards et al. (2006) assumed a flattening of the QLF at $z > 2.4$, motivated by the flatter $4 < z < 5$ QLF of Fan et al. (2001), which has since been shown to be incorrect (McGreer et al. 2013) and an artifact of a rapidly evolving break luminosity (see also Assef et al. 2011). The QLF of Ross et al. (2013) is only defined over the redshift range $2.2 < z < 3.5$, so we extrapolate the parameters using their functional form to the modestly larger $2 < z < 4$ range of Hot DOGs.

Let $\Phi(M_J, z)$ be the space density of QSOs at redshift z with absolute magnitude M_J. The number surface density of QSOs in the sky that are brighter than a certain luminosity in the redshift range $2 < z < 4$ is then given by

$$N_{\rm QSO} = \int_2^4 \int_{-\infty}^{M_J} \phi(M_J, z) \frac{dV_C}{dz} dM_J dz, \qquad (8)$$

where V_C is the comoving volume. The luminosity functions of Richards et al. (2006) and Ross et al. (2013) are parametrized as a function of $M_{i'}$, the absolute magnitude in the i'-band, which corresponds to the SDSS i-band shifted to $z = 2$. We use the rest-frame AB color of a Type 1 QSO with no host-contamination of $i' - J = -0.78$ determined by Assef et al. (2011) to convert between the absolute i' and J-band magnitudes. Figure 9 shows the cumulative surface density of Type 1 QSOs according to each of the QLF parametrizations. Each of the uncertainty regions shown in Figure 9 are estimated by calculating 500 realizations of the QLF created through re-sampling of each of its parameters according to their published 1σ uncertainties and assuming Gaussian statistics. The shaded regions show the 68% confidence interval of the 500 realizations. Note that as the co-variances between parameters are neglected, the uncertainty regions could be somewhat overestimated.

Figure 9 shows that the counts we obtained for Hot DOGs are quite well matched at the bright end by those predicted by the QLF of Ross et al. (2013), suggesting that Hot DOGs are as common as QSOs of comparable luminosity. This is roughly consistent with the comparison to the Assef et al. (2011) QLF except in the highest redshift range, where error bars are quite large due to the small size of the NDWFS Boötes field. Unsurprisingly, there is a significant discrepancy with the Richards et al. (2006) QLF, consistent with the large discrepancy between the latter and the Ross et al. (2013) QLFs. Also note that the optical color selection function of Richards et al. (2006) is least effective at $z \sim 2.5$

due to confusion with the colors of the stellar locus (Fan 1999). The difference in the faint-end of the slopes of the respective curves at $2.0 < z < 2.5$ may also suggest that Hot DOGs follow a different luminosity function than QSOs, although this is not observed in the higher redshift bins.

Some studies of lower-luminosity QSOs have found that the fraction of Type 2 AGN decreases strongly as a function of increasing bolometric luminosity (see, e.g., Ueda et al. 2003; Hasinger 2004; Simpson 2005; Assef et al. 2013), implying there should be a very small number of obscured QSOs at the luminosities of Hot DOGs. This prediction is significantly at odds with the results shown in Figure 9, since Hot DOGs appear to be as common as comparably luminous Type-1 QSOs. This discrepancy could indicate a reversal in the trends found at lower luminosities, implying that the fraction of Type-2 QSOs increases with luminosity towards the upper end of the QLF. Such a reversal has also been suggested by Banerji et al. (2012), although with limited statistics, based on the obscuration fraction of NIR selected QSOs. Banerji et al. (2012) suggests that these reddened, high luminosity QSOs may probe an evolutionary phase rather than an orientation effect. Other studies, primarily at lower luminosities, have found that the obscuration fraction may be a shallow function of the bolometric luminosity (Lusso et al. 2013) or independent of it (e.g., Wang & Jiang 2006; Hönig et al. 2011; Lawrence & Elvis 2010; Lacy et al. 2013), so that a high fraction of obscured QSOs at high luminosities may not be surprising. The obscuration of the lower-luminosity QSOs is thought to come from dust primarily in the vicinity of the SMBH, namely the dust torus, and models that replicate the lowering fraction of obscured objects with increasing luminosity have been devised for these structures (see, e.g., Lawrence 1991; Simpson 2005). This, however, may not be the case for Hot DOGs, which may be obscured by a different dust structure, such as dust on significantly larger physical scales or with a significantly different geometry or covering fraction, although we caution the reader that a significantly different covering fraction/geometry than that implied by our AGN SED template could have a considerable effect over the estimated M_J value (see also the discussion in §3). This could naturally solve the tension with the obscuration trends found for the lower-luminosity QSOs, and would imply that Hot DOGs are not the torus-obscured counterparts of the known Type 1 QSOs of similar luminosities. Lonsdale et al. (in prep.) have come to a similar conclusion for objects that may be the radio-loud counterparts of Hot DOGs. Measuring the total dust content from a combination of mid-IR and ALMA sub-mm observations, Lonsdale et al. (in prep.) suggests the torii of these objects would have to be unrealistically large to explain the high luminosities observed.

Alternatively, we could consider the possibility discussed in the previous section that the AGN in Hot DOGs radiate at an Eddington ratio significantly above unity, in contrast to typical $z \sim 2$ QSOs which radiate at $\lambda_E \sim 0.30$ (Kollmeier et al. 2006). We can speculate then that Hot DOGs are objects going through a phase of their evolution in which, for a brief period of time, they radiate well above their Eddington limit. If so, we should compare their number density to that of lower luminosity QSOs instead. In this case, we would conclude that Hot DOGs only constitute a small fraction of SMBHs of moderate to high mass, rather than a large fraction of the tip of the SMBH mass function. The fraction of QSOs of the same SMBH mass that are in this "Hot DOG phase" would constrain the duration of the latter relative to the QSO lifetime, and could be discussed in the context of the timescales estimated at the end of §4.2. We, however, refrain from exploring this any further here since there are too many uncertainties for a meaningful discussion.

As noted in §2.2.3, 30% of objects targeted for spectroscopy did not yield a successful redshift measurement, primarily due to optical faintness (Eisenhardt et al. in prep.). This means that while we considered 58 core sample W12drops with spectroscopic z and *Warm Spitzer* imaging, 83 were targeted. Their optical faintness implies the 25 additional objects have high-z, and here we have assumed they follow the same redshift distribution of Figure 1. The effects of a different redshift distribution can be approximated by modifying f_z, but is unlikely to qualitatively modify our conclusions. For example, if all of these 25 objects had $2 < z < 4$ and had the same magnitude distribution, the effects over the $2 < z < 4$ number density distribution of Figure 9 (top left panel)can be approximated by making $f_z = ((58 + 25)/252) \times (42/(42 + 25)) = 0.21$ instead of $f_z = 0.23$. Alternatively, in the unlikely scenario that all 25 objects had $z < 2$, we could approximate the effects by making $fz = 83/252 = 0.33$.

6. THE ENVIRONMENT OF HOT DOGS

Recently, Jones et al. (2014) found evidence of an overdensity of sub-mm neighbors to a small sample of Hot DOGs using 850μm observations with SCUBA-2 at JCMT, and also noted that the overdensity did not show an angular dependence around the Hot DOGs within $90''$. Assessing the environments of these objects is, however, not trivial, as their high redshifts and corresponding faintness makes getting spectroscopic distances a daunting task. Hence, we must rely on a statistical approach.

We use the deep *Warm Spitzer*/IRAC imaging described in §2.2.1 to count the number of galaxies neighboring Hot DOGs. Of the 96 Hot DOGs (see Table 1), we use the 90 that were observed as part of the same snapshot program (ID 70162; see Griffith et al. 2012, for details). Such imaging is ideal for this as the peak of the stellar emission is redshifted into the IRAC bands at the distance of Hot DOGs, allowing us to probe much lower stellar masses than what, for example, optical imaging would allow us to. We follow the approach of Wylezalek et al. (2013), and use the IRAC imaging to study the field density in the vicinity of Hot DOGs in comparison with the field density in two control samples: i) around random pointings in the *Warm Spitzer* UKIDSS Ultra Deep Survey (SpUDS, P.I.:J. Dunlop) representative of field galaxies, and ii) around radio-loud AGN in the Clusters Around Radio-Loud AGN survey (CARLA; Wylezalek et al. 2013, 2014; and see Galametz et al. 2010, 2013 for spectroscopic confirmation of two of these clusters). CARLA identifies moderately massive clusters at high redshift.

We start by counting for each of the 90 Hot DOGs the number of red galaxies ([3.6]–[4.5]>0.37, to select only $z \gtrsim 1$ galaxies) found in a $1'$ radius around it. We

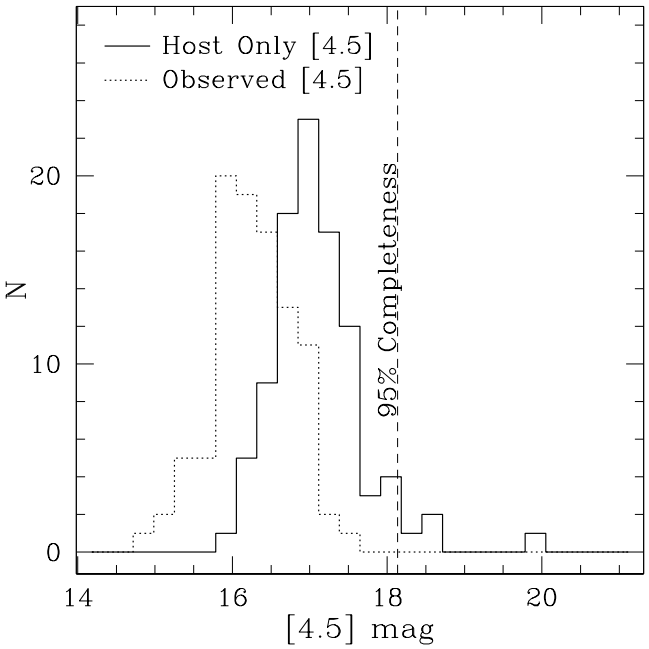

Figure 10. The solid line shows the distribution of the host galaxy observed-frame [4.5] magnitudes, obtained from the SED modeling described in §3. For comparison, the dotted line shows the observed [4.5] magnitudes, including the contribution of the AGN. The vertical dashed line shows the 10μJy completeness limit of our IRAC imaging.

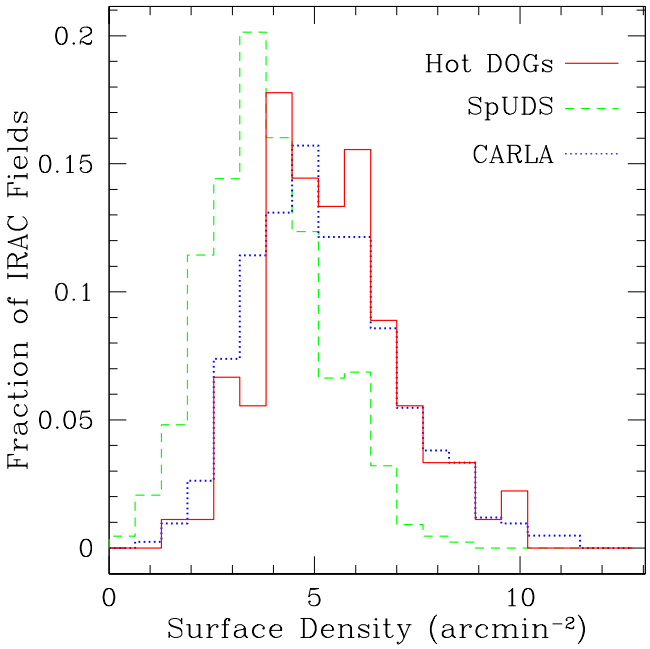

Figure 11. The solid red histogram shows the fraction of Hot DOGs with a given number density of objects brighter than 10μJy at [4.5] and with [3.6]-[4.5]>0.37 within 1′. We only consider Hot DOGs with IRAC observations and a reliable spectroscopic redshift. For comparison, we also show the distribution for all objects in the CARLA survey (*dotted blue histogram*) and for a sample of randomly selected positions in the SpUDS survey (*dashed green histogram*). The Hot DOG fields are overly dense compared to the random field, and similar to the CARLA fields.

use a circle with a 1′ radius because such size is small enough to fit well within a *Spitzer*/IRAC image, but large enough to encompass a typical mid-IR selected cluster with $\log(M_{200}/M_{\odot}) \sim 14$ at $z > 1$ (Brodwin et al. 2011; Wylezalek et al. 2013). We then repeat this around all 420 CARLA radio-loud AGN (RLAGN) and in 437 randomly selected pointings within the SpUDS survey. We determined that a grid of 19×23=437 apertures maximized the number of independent 1′ radii apertures extracted from the SpUDS survey region. The shallowest IRAC depth of the three samples is that of Hot DOGs, with a limiting [4.5] flux of 10μJy, so we only consider objects down to that depth in all three samples. We note that the [4.5] magnitudes of the host galaxies in Hot DOGs, obtained from the SED modeling described in §3, are typically $\sim$ 1 mag brighter than the 10μJy depth of our IRAC imaging, as shown in Figure 10.

Figure 11 shows the results of this analysis. The density of galaxies in the Hot DOG imaging is greater than that in the SpUDS control sample, suggesting the environment of Hot DOGs is significantly more dense than that of field galaxies. The Hot DOGs show good agreement with the CARLA sources, suggesting that Hot DOGs live in environments similar to those of RLAGN. Formally, a K-S test shows that the probability of the Hot DOG surface density distribution being drawn from the same parent population as that of the random pointings on the SpUDS survey field is 1.2×10^{-10}, while the probability raises to 0.69 when comparing with CARLA. The agreement with the CARLA survey fields is unexpectedly good, and leads to the speculation of whether Hot DOGs could be the precursors of RLAGN. In a follow-up work we will study in depth the radio properties of Hot DOGs, and explore this suggestion further (Tsai et al. in prep.).

As discussed earlier, one of the key assumptions of our SED analysis is that little to no obscuration is present in Hot DOG host galaxies. Under significant obscuration, Hot DOG stellar masses could be considerably larger and affect the interpretation of the results presented in §4. We note, however, that the stellar masses estimated by De Breuck et al. (2010) for RLAGN in CARLA clusters, likely the most massive members of the respective clusters, are not significantly above our upper bound estimates for Hot DOGs. If the upper bounds were underestimated due to unrecognized stellar obscuration, Hot DOGs would be expected to live in considerably denser environments.

To illustrate this point, we note that a study of the luminosity function of clusters in CARLA, has shown that at redshifts between $2.6 < z < 3$, their [4.5] luminosity function is consistent with a Schechter function with best-fit values of $\alpha = -1.28^{+0.15}_{-0.10}$ and $m^{*}_{[4.5]} = 19.59^{+0.25}_{-0.25}$ (Wylezalek et al. 2014). Using this luminosity function, we can estimate a lower bound on the expected number of galaxies brighter than 10μJy in a cluster containing a given Hot DOG by assuming the Hot DOG is the brightest cluster galaxy. When we consider all Hot DOGs with IRAC imaging, we find a marginal agreement between our predicted field densities and observed density distribution of the Hot DOG fields, with a K-S probability of 0.19 that both are drawn from the same parent population. Yet, if we assume that fluxes (hence stellar masses) are underestimated by a factor as small as 1.5, the K-S

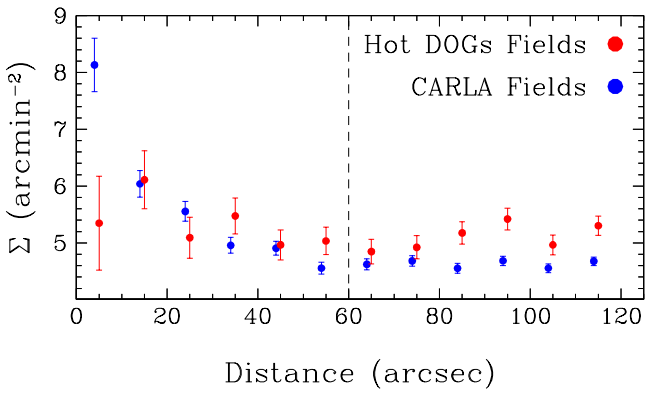

Figure 12. Differential surface density distribution, Σ, of red galaxies surrounding Hot DOGs (*red*) and CARLA RLAGNs (*blue*) as a function of the distance. The black dashed vertical line shows the distance considered for estimating the surface densities shown in Figure 11. The points from the CARLA fields have been offset by 1″ to the left for clarity. Compared to the CARLA fields, the environments around Hot DOGs are significantly less concentrated, despite the fact that the number density of galaxies within 1′ are similar. This is consistent with the low angular concentration in Hot DOG fields found by Jones et al. (2014) at 850μm.

probability decreases to 6×10^{-7}.

We conclude from these results that while Hot DOGs may live in dense environments, their field densities are inconsistent with clusters that host galaxies more massive than the upper bound stellar masses we estimated for them in §3. This reinforces our assumption of little to no host galaxy obscuration and shows that systematically underestimated stellar masses are not the drivers of the results discussed in §4.1 and §4.2.

Additionally, we can use the IRAC images to look at the concentration of galaxies in the vicinity of Hot DOGs. To do this we measure the angular surface density, Σ, of red galaxies (again selected as objects with [3.6]–[4.5]>0.37 and $f_{[4.5]} > 10$ μJy), in the fields of Hot DOGs as a function of the distance to the given Hot DOG. The results are shown in Figure 12. For comparison, we repeat the process in the CARLA fields, centered on the RLAGN targeted by the survey. We note the redshift distribution of CARLA RLAGN is quite similar to that of Hot DOGs. Compared to the CARLA fields, the environments around Hot DOGs are significantly less concentrated, despite the fact that the number density of galaxies within 1′ are similar. Such a difference could imply that Hot DOGs live in very dense filaments, or possibly in clusters that are in an earlier state of virialization. Alternatively, such results could be interpreted as Hot DOGs living in clusters as dense or denser than those found by CARLA, but that the Hot DOGs are not the central galaxy of the cluster. This is, however, unlikely, in light of the argument presented earlier based on the cluster luminosity function. We note this low angular concentration is consistent with the results of Jones et al. (2014) at 850μm within a similar radial distance of Hot DOGs.

7. CONCLUSIONS

We have presented a detailed study of the observed near-IR through mid-IR SEDs of a large set of Hot DOGs identified by WISE, focusing on the subsample with W4<7.2 (the core sample). Using the SED templates of Assef et al. (2010), we find that Hot DOGs are generally well fit by a combination of a luminous and obscured AGN that dominates the emission at rest-frame wavelengths $\lambda \gtrsim 1\mu$m, and a host galaxy that dominates the bluer emission. The AGN in Hot DOGs are among the most luminous AGN known and dominate the bolometric luminosity of these objects, accounting for >97% of the total $0.1 - 30\mu$m output in all objects.

Using these SED models, we find that the AGN in Hot DOGs display a large range of obscurations, with $2.5 < E(B-V) < 21.5$, and a mean of $\langle E(B-V) \rangle = 6.8$ (6.4) in the core (general) sample. Using the median dust-to-gas ratio in AGN of Maiolino et al. (2001), $E(B-V)/N_{\rm H} = 1.5 \times 10^{-23}$ cm^2 mag, these obscurations correspond to gas column densities of $1.7 \times 10^{23} < N_{\rm H} < 1.4 \times 10^{24}$ cm^{-2}, or over 10 times the 10^{22} cm^{-2} column used to separate Type 1 and Type 2 AGN, reaching into the Compton-thick regime. While significant host galaxy obscuration is unlikely, such obscuration would make us underestimate the dust absorption towards the accretion disk.

We estimate upper bounds on the stellar mass of Hot DOGs using the rest-frame K-band luminosities of the modeled host-galaxy component. These range from $11 < \log M_*/M_\odot < 12.5$, implying Hot DOGs could be some of the most massive galaxies at their redshifts. It is unlikely these upper bounds are underestimated, because the environmental densities of Hot DOGs are inconsistent with those needed to host more massive galaxies at their redshifts (see §6).

We investigated two approaches to estimate $M_{\rm BH}$ in Hot DOGs. If we assume the AGN in Hot DOGs radiate at the same λ_E of similar redshift QSOs, then Hot DOGs must deviate significantly from the local $M_{\rm Sph} - M_{\rm BH}$ relation. Such deviations are also observed for high redshift QSOs, and imply that the SMBH is assembled considerably before the stellar mass, constraining our current galaxy evolution models. Alternatively, we can estimate $M_{\rm BH}$ by assuming Hot DOGs follow the local $M_{\rm Sph} - M_{\rm BH}$ relation, and derive a minimum λ_E for these objects. If this is the case, AGN in Hot DOGs must be radiating at significantly super-Eddington ratios. This could imply that Hot DOGs could be at the transition point where the AGN is possibly expelling gas from the galaxy and quenching their star-formation, a scenario that may be consistent with the high fraction of extended Lyα emission found by Bridge et al. (2013).

We show in §5 that although very rare, the number density of Hot DOGs is comparable to that of equally luminous Type 1 AGN in the redshift range $2 < z < 4$. This suggests that Hot DOGs may not be the torus-obscured counterpart of the equally luminous Type 1 AGN, as the dust torus obscuration fraction is expected to be exceedingly small at these luminosities (e.g., Lawrence 1991; Simpson 2005; Assef et al. 2013). Considering the large Eddington ratios we estimate for these objects, we speculate that Hot DOGs may host AGN with significantly less massive SMBHs than the equally luminous Type 1 AGN, but that they are going through a phase where their accretion rates are temporarily enhanced, possibly to the point of quenching star-formation. In this scenario, when radiating at

their "normal" Eddington ratios, the AGN in Hot DOGs would constitute a small fraction of the Type 1 AGN with comparable mass SMBHs.

Finally, in §6 we study the environments of Hot DOGs using follow-up IRAC imaging. We show that the number of galaxies within a $1'$ radius is significantly above the number observed in random pointings implying Hot DOGs live in dense environments. Furthermore, we show that the environments are as dense as those of the clusters identified by the CARLA survey.

Further constraints on the host galaxy properties will allow us to better place these objects in the galaxy evolution context. The physical properties we have been able to determine here highlight how unusual Hot DOGs are among the general galaxy population or even other previously identified extreme populations (e.g., SMGs), and suggest that they may represent a pivotal transition in the galaxy evolution paradigm.

We are indebted to all WISE team members. We thank the anonymous referee for comments and suggestions that helped to improve this article. RJA was supported by Gemini-CONICYT grant number 32120009. This publication makes use of data products from the Wide-field Infrared Survey Explorer, which is a joint project of the University of California, Los Angeles, and the Jet Propulsion Laboratory/California Institute of Technology, funded by the National Aeronautics and Space Administration. This work is based in part on observations made with the *Spitzer Space Telescope*, which is operated by the Jet Propulsion Laboratory, California Institute of Technology under a contract with NASA. Kitt Peak National Observatory and Cerro Tololo Inter-American Observatory, National Optical Astronomy Observatory, are operated by the Association of Universities for Research in Astronomy (AURA) under cooperative agreement with the National Science Foundation. The WIYN Observatory is a joint facility of the University of Wisconsin-Madison, Indiana University, Yale University, and the National Optical Astronomy Observatory. The SOAR Telescope is a joint project of: Conselho Nacional de Pesquisas Científicas e Tecnológicas CNPq-Brazil, The University of North Carolina at Chapel Hill, Michigan State University, and the National Optical Astronomy Observatory. Based partly on observations obtained at the Hale Telescope, Palomar Observatory as part of a continuing collaboration between the California Institute of Technology, NASA/JPL, NOAO, Oxford University, Stony Brook University, and the National Astronomical Observatories of China.

Facilities: WISE, Spitzer (IRAC), Hale (WIRC), MMT (SWIRC), SOAR (OSIRIS), WIYN (WHIRC)

REFERENCES

Assef, R. J., et al. 2010, ApJ, 713, 970
—. 2011, ApJ, 728, 56
—. 2013, ApJ, 772, 26
Baldry, I. K., Glazebrook, K., & Driver, S. P. 2008, MNRAS, 388, 945
Banerji, M., McMahon, R. G., Hewett, P. C., et al. 2012, MNRAS, 427, 2275
Bennert, V. N., Auger, M. W., Treu, T., Woo, J.-H., & Malkan, M. A. 2011a, ApJ, 726, 59
—. 2011b, ApJ, 742, 107
Bentz, M. C., Peterson, B. M., Pogge, R. W., & Vestergaard, M. 2009, ApJ, 694, L166
Blain, A. W., Smail, I., Ivison, R. J., Kneib, J.-P., & Frayer, D. T. 2002, Phys. Rep., 369, 111
Bongiorno, A., Maiolino, R., Brusa, M., et al. 2014, MNRAS, 443, 2077
Borys, C., Smail, I., Chapman, S. C., Blain, A. W., Alexander, D. M., & Ivison, R. J. 2005, ApJ, 635, 853
Bridge, C. R., et al. 2013, ApJ, 769, 91
Brodwin, M., et al. 2011, ApJ, 732, 33
Brown, W. R., McLeod, B. A., Geary, J. C., & Bowsher, E. C. 2008, Proc. SPIE, 7014,
Brown, M. J. I., Moustakas, J., Smith, J.-D. T., et al. 2014, ApJS, 212, 18
Bruzual, G., & Charlot, S. 2003, MNRAS, 344, 1000
Cardelli, J. A., Clayton, G. C., & Mathis, J. S. 1989, ApJ, 345, 245
Casey, C. M., Narayanan, D., & Cooray, A. 2014, Phys. Rep., accepted (arXiv:1402.1456)
Chabrier, G. 2003, PASP, 115, 763
Conroy, C., Dutton, A. A., Graves, G. J., Mendel, J. T., & van Dokkum, P. G. 2013, ApJ, 776, L26
Conroy, C., & Gunn, J. E. 2010, ApJ, 712, 833
Conroy, C., Gunn, J. E., & White, M. 2009, ApJ, 699, 486
Coppin, K. E. K., et al. 2008, MNRAS, 389, 45
Croton, D. J., et al. 2006, MNRAS, 365, 11
Depoy, D. L., Atwood, B., Byard, P. L., Frogel, J., & O'Brien, T. P. 1993, in Society of Photo-Optical Instrumentation Engineers (SPIE) Conference Series, Vol. 1946, Infrared Detectors and Instrumentation, ed. A. M. Fowler, 667–672
De Breuck, C., Seymour, N., Stern, D., et al. 2010, ApJ, 725, 36
Dey, A., et al. 2008, ApJ, 677, 943
Eisenhardt, P. R. M., et al. 2012, ApJ, 755, 173
—. in prep.
Elvis, M., et al. 1994, ApJS, 95, 1
Faber, S. M., et al. 2007, ApJ, 665, 265
Fan, X. 1999, AJ, 117, 2528
Fan, X., et al. 2001, AJ, 121, 54
Fazio, G. G., et al. 2004, ApJS, 154, 10
Ferrarese, L., & Merritt, D. 2000, ApJ, 539, L9
Galametz, A., Stern, D., Stanford, S. A., De Breuck, C., Vernet, J., Griffith, R. L., & Harrison, F. A. 2010, A&A, 516, A101
Galametz, A., et al. 2013, A&A, 559, A2
Gordon, K. D., & Clayton, G. C. 1998, ApJ, 500, 816
Griffith, R. L., et al. 2012, AJ, 144, 148
Gültekin, K., et al. 2009, ApJ, 698, 198
Hasinger, G. 2004, Nuclear Physics B Proceedings Supplements, 132, 86
Hönig, S. F., Leipski, C., Antonucci, R., & Haas, M. 2011, ApJ, 736, 26
Hopkins, P. F., Hernquist, L., Cox, T. J., & Kereš, D. 2008, ApJS, 175, 356
Jahnke, K., & Macciò, A. V. 2011, ApJ, 734, 92
Jarrett, T. H., et al. 2011, ApJ, 735, 112
Jones, S., et al. in prep.
Jones, S. F., et al. 2014, MNRAS, 443, 146
Kaspi, S., Smith, P. S., Netzer, H., et al. 2000, ApJ, 533, 631
Kochanek, C. S., Khan, R., & Dai, X. 2012, ApJ, 759, 20
Kollmeier, J. A., et al. 2006, ApJ, 648, 128
Lacy, M., Ridgway, S. E., Gates, E. L., et al. 2013, ApJS, 208, 24
Lake, S. E., Wright, E. L., Cutri, R. M., & Eisenhardt, P. R. 2013, in American Astronomical Society Meeting Abstracts, Vol. 221, American Astronomical Society Meeting Abstracts, #443.09
Lawrence, A. 1991, MNRAS, 252, 586
Lawrence, A., & Elvis, M. 2010, ApJ, 714, 561
Lonsdale, C., et al. in prep.
Lusso, E., Hennawi, J. F., Comastri, A., et al. 2013, ApJ, 777, 86
Magorrian, J., et al. 1998, AJ, 115, 2285
Mainzer, A., et al. 2011, ApJ, 731, 53
Maiolino, R., Marconi, A., Salvati, M., Risaliti, G., Severgnini, P., Oliva, E., La Franca, F., & Vanzi, L. 2001, A&A, 365, 28
Mancone, C. L., & Gonzalez, A. H. 2012, PASP, 124, 606
Maraston, C. 2005, MNRAS, 362, 799
Marconi, A., & Hunt, L. K. 2003, ApJ, 589, L21
McGreer, I. D., et al. 2013, ApJ, 768, 105
Meixner, M., et al. 2010, PASP, 122, 451
Peng, C. Y. 2007, ApJ, 671, 1098

Richards, G. T., et al. 2006, AJ, 131, 2766
Roseboom, I. G., Lawrence, A., Elvis, M., et al. 2013, MNRAS, 429, 1494
Ross, N. P., et al. 2013, ApJ, 773, 14
Sanders, D. B., & Mirabel, I. F. 1996, ARA&A, 34, 749
Schmidt, M. 1968, ApJ, 151, 393
Shen, Y., Greene, J. E., Strauss, M. A., Richards, G. T., & Schneider, D. P. 2008, ApJ, 680, 169
Simpson, C. 2005, MNRAS, 360, 565
Skrutskie, M. F., et al. 2006, AJ, 131, 1163
Stern, D., et al. 2014, ApJ, 794, 102
Thompson, T. A., Quataert, E., & Murray, N. 2005, ApJ, 630, 167
Trainor, R., & Steidel, C. C. 2013, ApJ, 775, L3
Tremaine, S., et al. 2002, ApJ, 574, 740
Tsai, C.-W., et al. 2014, ApJ, submitted (arXiv:1410.1751)
Tsai, C.-W., et al. in prep.
Ueda, Y., Akiyama, M., Ohta, K., & Miyaji, T. 2003, ApJ, 598, 886
Vestergaard, M., & Peterson, B. M. 2006, ApJ, 641, 689
Wang, J. X., & Jiang, P. 2006, ApJ, 646, L103
Wang, R., et al. 2010, ApJ, 714, 699
Werner, M. W., et al. 2004, ApJS, 154, 1
Wilson, J. C., et al. 2003, in Society of Photo-Optical Instrumentation Engineers (SPIE) Conference Series, Vol. 4841, Instrument Design and Performance for Optical/Infrared Ground-based Telescopes, ed. M. Iye & A. F. M. Moorwood, 451–458
Wright, E. L., et al. 2010, AJ, 140, 1868
Wu, J., et al. 2012, ApJ, 756, 96
—. 2014, ApJ, accepted (arXiv:1405.1147)
—. in prep.
Wylezalek, D., et al. 2013, ApJ, 769, 79
—. 2014, ApJ, 786, 17
York, D. G., et al. 2006, MNRAS, 367, 945